CARBON 59 (2013) 130–139

Available at www.sciencedirect.com

SciVerse ScienceDirect

journal homepage: www.elsevier.com/locate/carbon

An electrochemical approach to fabricating honeycomb assemblies from multiwall carbon nanotubes

Jigang Zhou [a,d], *Hao Liu* [b], *Fengping Wang* [a,e], *Todd Simpson* [c], *Tsun-Kong Sham* [a], *Xueliang Sun* [b], *Zhifeng Ding* [a,*]

[a] *Department of Chemistry, The University of Western Ontario, London, ON, Canada N6A 5B7*
[b] *Department of Mechanical and Materials Engineering, The University of Western Ontario, London, ON, Canada N6A 5B7*
[c] *Nanofabrication Facility, The University of Western Ontario, London, ON, Canada N6A 5B7*
[d] *Canadian Light Source Inc., Saskatoon, SK, Canada S7N 0X4*
[e] *Department of Physics, University of Science and Technology Beijing, Beijing 100083, China*

ARTICLE INFO

Article history:
Received 30 September 2012
Accepted 2 March 2013
Available online 13 March 2013

ABSTRACT

We report a method for controllably fabricating a structurally stable array of multiwall carbon nanotubes (MWCNTs) with greatly enhanced surface area for catalyst loading as compared with a vertically aligned MWCNT forest. These structures may provide increased electrocatalytic activity for methanol oxidation reactions and oxygen reduction reactions in fuel cells. Potentiodynamic pretreatment is shown to allow the controlled restructuring of a vertically aligned MWCNT forest on a silicon substrate into walled domains of honeycomb-like polygons. Electrochemical parameters, such as the potential scanning ranges and cycles, were found to be capable of tuning the carbon nanotube surface interaction with a solvent and thereby the density and homogeneity of walled-domains that form under solvent dilation stress. Confocal Raman microspectroscopy with a spatial resolution of 200 nm was used to characterize these assemblies along with scanning electron microscopy and X-ray absorption spectroscopy. The MWCNTs in general retained their pristine structural characteristics except in places where they were bent, which showed a slightly reduced wall thickness.

1. Introduction

Carbon nanotubes (CNTs) exhibit super mechanical strength [1], high chemical stability [2] and attractive structure dependent electronic properties [3]. As with their counterpart graphene [4], the assembly of CNTs into desired structures or arrangements such as arrays [5] with controlled shape, orientation and density, is required for nanoscale device applications [6]. CNT assembly can be performed during synthesis (chemical) or post-synthesis (chemical and physical). Although more challenging, post-synthesis modification allows processing flexibility and enables unique testing systems that provide physical insight into the proximity effect of nanostructures. In comparison to the well-documented plasma and strong acid oxidation methods, electrochemical treatments of CNTs in purification and manipulation processes [7,8] provide advantages under mild reaction conditions with high efficiency and good controllability.

Three dimensional honeycomb-like CNT structures have been formed by spreading liquids into CNT forests [5,9–11], by evaporating liquid from the immersed CNT forests [12,13], and by direct assembly growth through pyrolysis of precursors [14]. In both post-synthesis approaches, the

* *Corresponding author:* Fax: +1 519 6613022.
E-mail address: zfding@uwo.ca (Z. Ding).
0008-6223/$ - see front matter
http://dx.doi.org/10.1016/j.carbon.2013.03.001

underlying mechanism is CNT adhesion and solvent dilation stress acting upon CNT bundles of different density. However, the surface properties required for the assembly are not clearly understood. Further, controllability and flexibility of the processes have not been explored in detail. Recently, electrochemical polarization has been demonstrated to enable wetting of CNT forests and the wicking of water through the superhydrophobic membrane [15]. The observed wetting phenomenon is attributed to the oxidation of CNTs surface by the electrochemistry process, where a positive dc potential of 1.7 V has been applied to CNTs.

Concurrently, we have developed a novel route to fabricate luminescent carbon nanocrystals (NCs) by electrochemically treating multiwall carbon nanotubes (MWCNTs) [7]. During the electrochemical treatment, the MWCNT morphology were deformed and further cut to small fragments through ultrasonication [16]. The electrochemical deformation of the MWCNTs was observed to be dependent on the duration of potential scanning. The MWCNT fragments from the above process also exhibit hydrophilic characteristics and form a super stable ethanol dispersion that lasts for months [16]. Those results motivate us to apply similar treatment to vertically aligned MWCNT forest structures. Herein we report on electrochemical treatment of a vertically aligned MWCNT forest on silicon wafer substrates immersed in an electrolyte solution of 0.1 M tetrabutylammonium perclorate (TBAP) in acetonitrile (MeCN). For the first time, walled domains of honeycomb-like polygons were formed from the electrochemically treated MWCNTs on the substrate upon evaporation of ethanol used to wash out the electrolyte solution residue. We show that adjusting potentiodynamic parameters such as the number and range of potential cycling can control the structure and quality of the CNT honeycombs. The honeycomb assembly thus prepared was investigated using confocal Raman microspectroscopy, X-ray absorption spectroscopy and scanning electron microscopy (SEM). Structural insights into CNT variations before and after the honeycomb formation were gained for the first time. The increased accessible CNT sidewall surface area is expected to enhance the electrocatalytic activity for methanol oxidation reactions and oxygen reduction reactions in fuel cells as sources of "green" power for automobiles and portable electronics [17–19]. In contrast to the well-controlled formation of three-dimensional polygons, pillars, and other CNT microstructures reported by Liu et al. [20] and Lim et al. [11] using laser-induced artificial patterns, our approach is simple, fast and will enable the low-cost fabrication of MWCNT honeycombs. It is anticipated that our preparative methodology could be utilized for increasing surface area and catalyst loading in fuel cell applications.

2. Experimental details

2.1. Synthesis of vertically aligned MWCNT forest on Si wafer

High density vertically aligned MWCNTs forests were produced following the floating catalyst method. The synthesis detail can be found in our previous publication [21]. In brief, 100 mg of ferrocene (98%, Aldrich, Mississauga, ON) was placed at the entrance of a furnace in the quartz tube. Argon (99.99% in purity, Aldrich) was first introduced into the system at room temperature at a flow rate of 500 sccm for 30 min to purge the air. The system was then heated to 800–900 °C and ethylene gas was introduced into the system at a flow rate of 10 sccm keeping the Ar flow rate unchanged. Thus the ferrocene vapor was carried by the gas flow into the high temperature section where the pyrolysis of ferrocene and growth of CNTs occurred on a silicon wafer pre-coated with a layer of conducting polymer. The whole system was kept at the target temperature for 5 min, then the ethylene gas was turned off and the system was cooled down to room temperature with the Ar gas flowing.

2.2. Fabricating CNT honeycomb structures

The CNT forest covered Si wafer was cut to a suitable size and was clamped in a custom-designed holder to ensure electric contact for electrochemistry and an exposed surface area of 0.3 cm^2 to the electrolyte solution. The electrochemical cell consisted of this working electrode, a Pt coil counter electrode, and a Ag quasi-reference electrode in acetonitrile (MeCN) containing 0.1 M of tetra-*n*-butylammonium perchlorate (TBAP) as the supporting electrolyte. The electrode potential could be calibrated by the known potential of ferrocenium/ferrocene (Fc^+/Fc) as 0.342 V versus standard calomel electrode (SCE) in the same system [16] The electrochemical treatment was performed by cycling the applied potential between −2.00 and 2.00 V, a potential range well within the potential window of this supporting electrolyte [22], at a scan rate of 0.5 V/s, using an electrochemical analyzer (CHI 601A, CH Instruments, Austin, TX). The treatment duration was described as potential cycles. The best structure was obtained with cycle number between 50 and 100. Long cycling (for instance, 1000 cycles) will remove all CNTs from the substrate.

After desired electrochemical cycles, the substrate with the treated CNT forest was removed from the solution and washed thoroughly using pure acetonitrile followed by ethanol. The material was then dried in air prior to analyses.

2.3. Characterization and manipulation of CNT honeycombs by SEM and focused ion beam (FIB)

The CNTs resulting from electrochemical treatment were examined by a LEO 1540XB FIB/SEM operated at 1–3 kV with a working distance (WD) of 4–6 mm. The prepared samples display a structure comprised of walled domains of honeycomb-like polygons. The cross-section of the CNT honeycombs was accomplished by milling the honeycomb with a focused gallium ion beam (FIB) of energy 30 keV. A rectangular region in the foreground of the cross section was milled with a 1 nA beam to remove some CNTs, which would otherwise block the view of the cross section. The milling rate was dramatically accelerated and redeposition minimized through the local injection of water vapour through a capillary directed at the milling region. The cross section was then polished with a 200 pA beam to remove approximately 1 μm of the newly exposed surface. During FIB milling, the ion beam

was incident normal to the sample surface and parallel to the exposed cross section. The cross section was then imaged by SEM with the sample tilted 54° from the surface normal. To examine the structure stability of the honeycomb, the rim of the honeycomb was cut by FIB with a 200 pA ion beam and grabbed by a nanomanipulator (Ascend Instruments, Extreme Access, Oregon).

2.4. Confocal Raman microspectroscopy

Confocal Raman microspectroscopy (Alpha-SNOM, WITec, Germany) was conducted under ambient conditions as reported elsewhere for single tin dioxide nanoribbons [23]. A YAG linearly polarized laser (Verdi 5, the Coherent Inc., Santa Barbara, CA) with a 532 nm wavelength was used for Raman excitation. A laser output power of 10 mW was selected for the experiments. A 50× objective with 0.75 NA (Nikon Canada, Mississauga, ON) was used to focus the laser beam onto the specimen and collect Raman signals. A complete Raman spectrum was recorded at each image pixel by an air-cooled (−70 °C), back-illuminated spectroscopic CCD (Model DV401-BV, ANDOR, UK) behind a grating (300 or 1800 g mm^{-1}) spectrograph (UHTS300, WITec). In general practice, Raman images were constructed by the integration of the intensities of characteristic Raman bands in a scan area with 256 × 256 pixels. One image includes 65536 spectra with an integration time of 100 ms per spectrum. Depth scanning images depicting chemical distribution in X–Z orientation were also conducted [7,23].

3. Results and discussion

3.1. Scanning electron microscopy of as-grown CNT forests

The as-grown vertically aligned MWCNTs were examined by SEM as shown in Fig. 1. The CNT forest consisted of vertically oriented MWCNTs with a mean diameter of 50 nm (Fig. 1a) and a height of 15 μm as determined from the side view of the CNT forest in Fig. 1b. It can be observed that the top of the MWCNT forest was not perfectly aligned. The bent CNT tips entangle together and render the forest surface rough. The interlocking MWCNT tips and the large interspace among CNTs due to the smaller diameter of the tip at the forest top are expected to improve the penetration of liquids into the CNT forest under electrochemical polarization.

3.2. Formation of honeycomb-like patterns and their mechanistic characterization

50 cycles of linear scans between −2.00 and 2.00 V at a scan rate of 0.5 V/s were applied to the MWCNT forest on Si substrate immersed in MeCN with 0.1 M TBAP as the supporting electrolyte. The CNT forest was then rinsed thoroughly by pure acetonitrile and ethanol in sequence.

The sample was then dried naturally in ambient atmosphere. SEM images of the obtained sample (Fig. 2) showed that the originally vertical MWCNT forest became a honeycomb-like assembly in an area as large as several square centimeter.

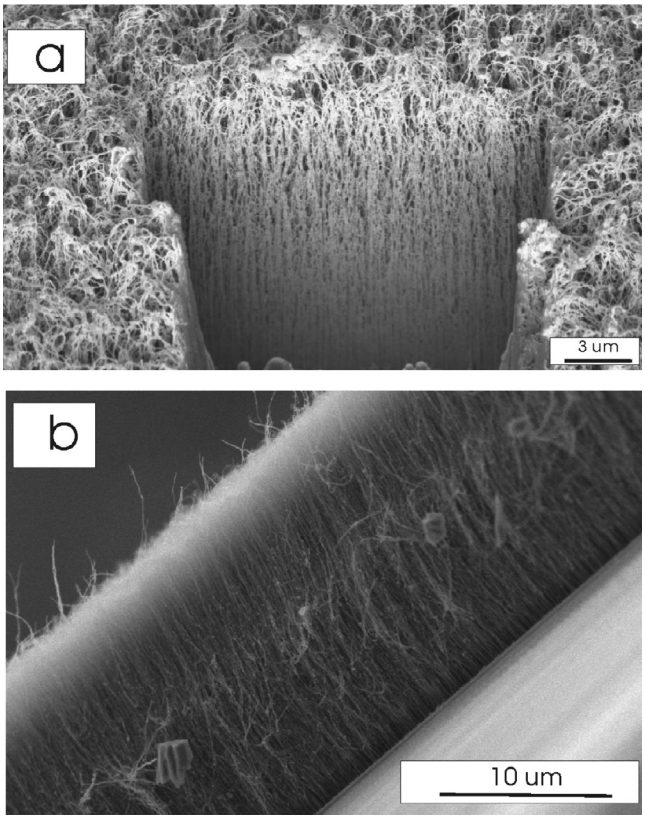

Fig. 1 – SEM images of a vertically aligned MWCNT forest on a Si substrate. (a) A top view of the CNT forest from a tilted angle with a rectangular cavity milled by focused ion beam. (b) A side view of the CNT forest.

Though CNT difference is not known between this work and previous works, our honeycombs can be distinguished from those observed by Chakrapani et al. and Liu et al. [10,13] by a couple of features: (1) while their structures showed polygonal network cells with average crack length greater than the average cell width, ours exhibited mainly hexagonal and pentagonal structures mixed with a few triangles, which serve as the transition regions between polygons; (2) the nominal diameters of our honeycomb-like cavities are in the range of 5–25 μm whereas theirs were several tens micrometer larger. From the geometry and size, our structures are expected better physical stability. Chakrapani et al.'s structures were formed by the assistance of oxidation in an oxygen plasma created in a glow discharge chamber, and Liu et al. employed a water droplet placed on the fresh CNT film, whilst ours were facilitated by electrochemistry.

The labyrinthine ridges are more compact than comb bodies, and are similar to basket rims (Fig. 2a). The rims of the cells were composed of compacted and bent MWCNTs as illustrated by the top inset of Fig. 2a. In Fig. 2b that is a tilting view of several combs, the rims of cavities were imaged to be almost perpendicular to the cavity bottom plane. The cells sloped upward, each with a center where the MWCNTs radiated out (Fig. 2b). The structure stability was checked in the

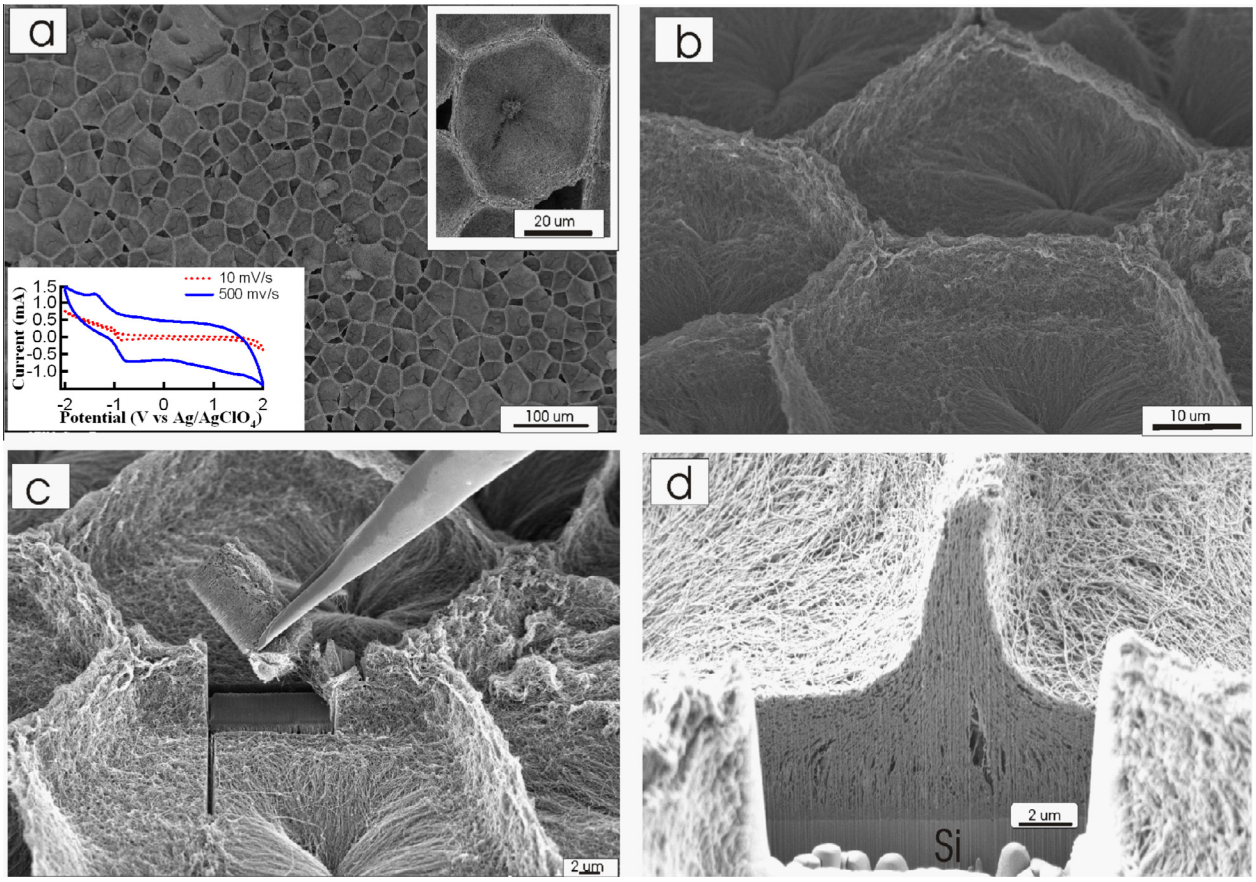

Fig. 2 – SEM images of honeycombs formed by CNT adhesion and solvent dilation stress exerting on the MWCNTs during the evaporation of the soaked liquid after 50 potential scanning cycles between −2.00 and 2.00 V. (a) A top view of the honeycombs with a top inset showing an enlarged comb and bottom inset manifesting cyclic voltammograms of MWCNTs on a Si substrate at scanning rates of 10 and 500 mV/s; (b) a top view of several cells from a tilted angle; (c) mechanical manipulation of a piece of comb rim after FIB milling; and (d) a side view of a ridge cross-section milled.

following sequence: (1) the honeycomb rim was cut by FIB milling; (2) a nanomanipulator was used to grab the cut rim; and (3) the rim was pulled away from the honeycomb. As shown in Fig. 2c, the shape of the rest of the cavity and the cut rim remained intact. This demonstrates that the honeycomb is robust. Considering that the intrinsic elasticity favors MWCNTs mechanically to be straight, there must have another force existed to bend CNTs in honeycombs. The structure stability of the deformed MWCNTs in the dried honeycomb structure suggests that the elasticity of the bent CNTs has been changed due to the weak links associated with the electrochemically produced defects, for instance oxygen bearing surface functional group. Furthermore, one single rectangular cavity was opened by FIB milling and the cross-section of the ridge was examined by SEM as shown in Fig. 2d. The rim thickness at the top was determined to be around 2 μm and the depth of the cavity was around 10 μm. The bending extent of the MWCNTs depended obviously on their location as well illustrated by the cross section SEM in Fig. 2d. While the CNTs right in the middle of the ridge were still vertically aligned, most MWCNT as shown in the cross section in Fig. 2d were bent to sigmoidal shapes. The end near the Si substrate kept vertically straight, but the CNT bottom middle bent to follow the stream of the assembly. The bending angle of the CNTs at the rim edge was increased to nearly 90°. This trend can be seen clearly from the CNT geometries demonstrated by high resolution SEM of the cross section in Fig. 2d. Since the CNT length was constant, the free end of these s-shaped MWCNT swirls reach different levels on the cell inner wall. Fig. 2d illustrates well how theses swirls constitute a cell from the cross-section view. The MWCNTs radiating from the center appear less dense than elsewhere and compose the deepest area in the cell. The centers were not necessary in the middle of the combs.

It is proposed that the CNT bending was dependent on the balance among capillary forces, the elasticity, density, length and entanglement of the CNTs. These interactions/features are similar to those in the coalescence process of parallel elastic lamellae such as a paint brush dunked into a wetting liquid [24]. The capillary forces should be contributed from the solvent dilation stress among the CNTs in a bundle [10] as well as adhesive force after solvent wetting [24]. As described by the SEM in Fig. 1, our CNT forest entangled at the top while the bottom part very similar to that of a brush was rigid due to the regular space kept by the substrate. In this context, the assembly of the CNTs was more complex than the brush hair coalescence because of this extra interaction. It also should be noticed that the formation of such

assembly also depends on the density, the length of the CNTs and the solvent used to wash out the electrolyte.

3.3. *Honeycomb assembly modulated by electrochemistry*

The electrochemical oxidation on the CNTs has been extensively investigated in the purification, functionalization and shortening of CNTs [8,25,26]. The electrochemically active locations in CNTs have been recognized to be associated with the edge-plane-like sites, such as the CNT tips or the defects along the CNT axis [27]. The graphitic characteristics in CNTs also favored ion and small molecule intercalation into the graphene interlayer along the CNTs walls [28,29]. We have discovered that the potential cycling between −2.00 and 2.00 V on CNTs in the electrolyte solution can deform randomly orienting CNTs effectively [16]. The deformed CNTs have been cut into small fragments with the hydrophilic characteristics with limited number of potential scanning [16]. When the potential applied to CNTs is in the positive region, the CNTs can be oxidized on the surface defect sites along the CNTs wall or at the open ends. The oxidation can also produce more defects and change the chemical feature in the reaction area.

In addition, the possibility of TBA^+ intercalation into the CNTs lattice through the defects along the tube axis was proposed [16]. Such intercalation in turn generated more disordered carbon structures on CNTs. To verify such hypothesis, the electrochemical response of the as-grown CNT forest on the silicon was examined by the cyclic voltammogram (CV) shown by the bottom inset in Fig. 2a. Similar to our previously reported results for CNTs in random orientation on carbon fiber papers [7], a large charging current was presented for the vertically aligned CNTs to the Si plane, which reveals the associated large electrochemical active area in CNTs. In addition to the large charging current, the oxidation peaks [7] can be identified. However, the oxidation currents are small relative to the charging current. Oxidation of CNTs could produce more defects that further enable electrochemical intercalations. Such electrochemical treatment will bring more surface defects and hydrophilicity on CNTs based on our previous investigation [16]. On the other hand, the reduction of oxygen at −1.20 V was found upon changing the polarity on the CNT forest. Other possible reactions in the negative potential region might be the reduction of the surface oxygen function groups, leading the CNT surface more hydrophobic. The intercalation of TBA^+ and acetonitrile into CNTs can not be excluded yet in this potential region. The above reduction and oxidation reactions might lead to wicking the MeCN through the CNT forest [15]. The other roles of the negative potential scanning in the process are not yet clear. To better understand the electrochemical treatment mechanism, we used lithium perchlorate and found no pattern formed following the same treatment procedure. This suggests that larger cations, like TBA^+, are essential in the treatment to form the pattern. The observation also demonstrates the important role of negative potential scanning in forming the honeycomb structure. It would be worthy to vary the counter ion in the tetraalkylammonium series to investigate the nature of the counter ion in the electrochemical assembly.

The potential cycling between negative and positive potential limits might leverage surface redox states and the oxygen functional groups [16], and therefore hydrophobicity and hydrophilicity on the CNTs. The initial potential sweep direction does not affect the treatment result. These surface state changes probably happened at the forest top, i.e. the tip of each individual CNT due to the electric field distribution. This fact enhanced the coalescence, which explained why the honeycomb rims possessed impacted structures. Inletting and soaking of solvents into the interspace of the CNTs was facilitated by applying voltage on the Si substrate, a phenomenon of electrophoresis. The soaked acetonitrile mixed with the washing ethanol, which applied the dilation stress to CNTs [10]. After wetting, the MWCNTs adhere each other. Both caused CNT bending.

After such treatment, the solvents can then be more efficiently soaked into the interspaces between treated CNTs due to the capillary force. Honeycomb assembly was observed after the evaporation of the solvents.

The morphological evolution of the CNT forest during electrochemical treatment was also investigated in situ by optical microscopy. The formation of the honeycombs was not observed, confirming that the structure does not form during the wetting and spreading phase but during the drying of liquid from CNT forest [13]. The complex hierarchical honeycomb structure results from the balance between surface tension and the mechanically elasticity of the CNTs [30].

3.4. *Control experiments*

To confirm that electrochemistry is essential to the formation of honeycombs, we examined the CNT forest after dipping in the various liquid and drying. The CNTs appeared to be bundled and formed cellular structures in such samples as shown in Fig. 3. However the cellular structures only existed in very limited areas. The rims of the cellular cavity were only loosely coalescence and the cells were also very shallow. The shallow cavity suggests that the drying of the liquid only works at the top of CNTs. The physical and chemical varieties in the

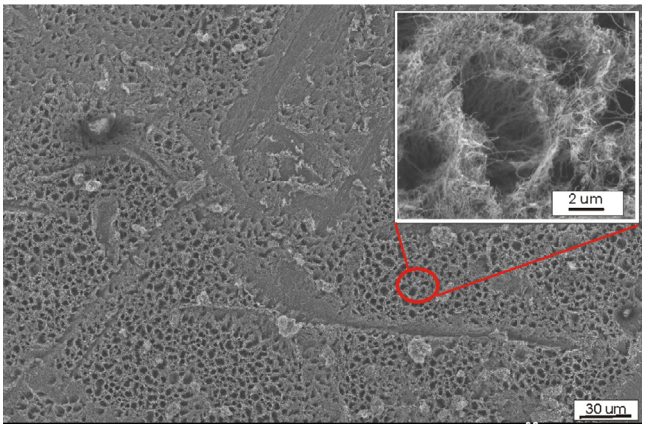

Fig. 3 – A SEM image of cellular structures formed from CNTs with the treatment sequence of dipping in the supporting electrolyte solution, washing with pure acetonitrile and ethanol, and drying as in Fig. 3. Inset is a zoomed-in area showing loose honeycombs formed without electrochemical treatment.

different locations of as-grown CNT forest are contributing factors for the formation of the cellular structure. The localized nature only allows for the formation of low quality cellular structures in the specific location without the electrochemical pretreatment of CNTs. It would be worthy to treat CNTs by other oxidation, for instance oxygen plasma treatment, and repeat the control experiment to examine the merits of our approach.

3.5. *Electrochemical modulation of honeycomb formation*

Potential scanning only in positive region or negative region was also examined. Fig. 4a shows that single directional potential scanning (positive or negative scanning alone) produces only weakly entangled honeycomb structures covering relative small areas. Wang et al. [15] discovered that water can be efficiently wet and pumped through superhydrophobic aligned MWCNT membranes upon a small positive dc bias of 1.7 V, with the membrane acting as anode. Combining our experiment results as described above, it is plausible that just positive applied potential could change the CNT wetability but is not sufficient for CNT assembling. Negative potential likely caused the reduction of surface oxygen functional groups [16] and cation interaction into CNT though the full mechanism requires further study. Nevertheless, well-defined honeycombs with consolidated rims are obtained if the CNTs are further cycled in both cathodic and anodic regions (Fig. 4b). It is proposed that alternating oxidation (positive scanning) and reduction (negative scanning) in sequence is the most efficient route to tailoring CNTs and the desired honeycomb structures that are produced during the evaporation of the solvent. In other words, the formation of honeycombs depends on the potential scanning and potential scanning direction. It is worth mentioning that the honeycomb structures formed in low quality can be modified and improved to higher quality by further electrochemical treatments. This observation further confirms that the obtained structure is a result of the electrochemical modifications combined with the capillary driving force exerting on the treated MWCNTs during the evaporation of the solvent.

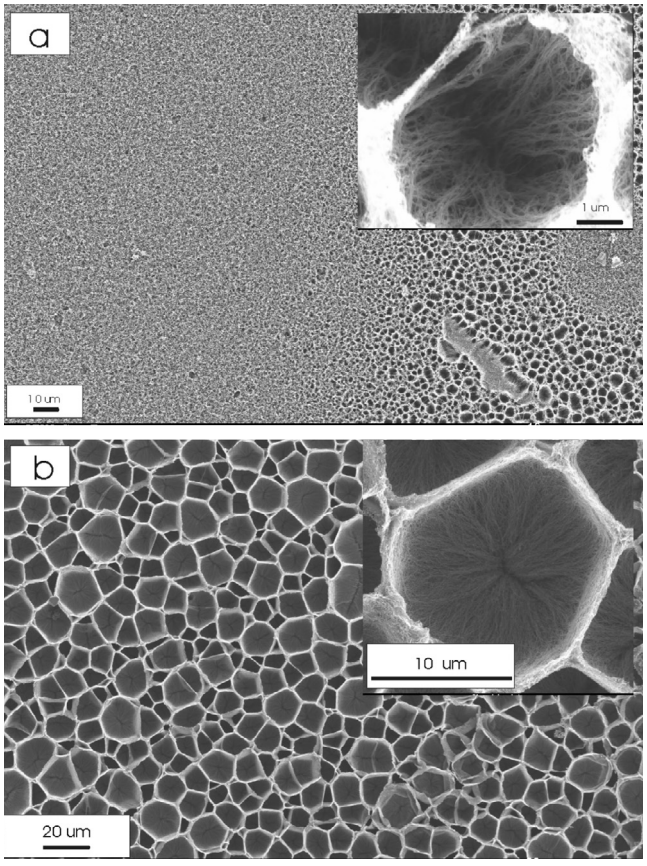

Fig. 4 – Comparison of honeycomb formed by capillary driving force exerting on the MWCNTs during the evaporation of the soaked liquid after 50 potential scanning cycles between 0.00 and 2.00 V (a) and between −2.00 and +2.00 V (b). Insets demonstrate a zoomed-in comb for each of the above two cases.

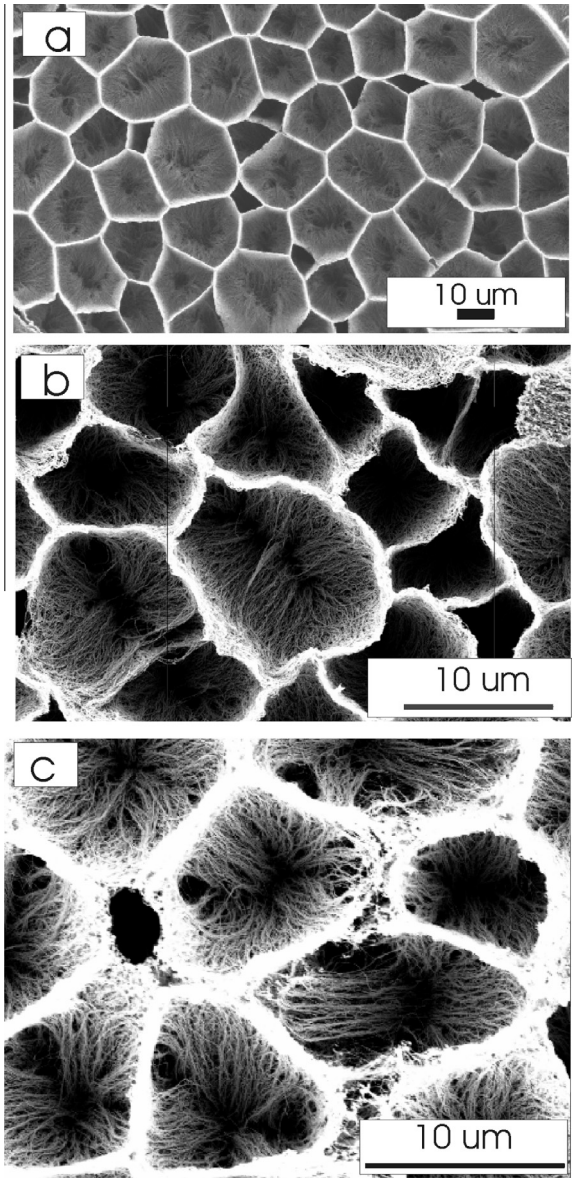

Fig. 5 – Comparison of honeycombs formed from CNTs electrochemically treated by potential scanning in the range of ±2.00 V (a), ±1.50 V (b), and ±1.00 V (c). Other conditions are the same as in Fig. 4.

Potential scanning range within the potential window of this supporting electrolyte was also found to be important in determining the final quality of the honeycombs. As shown in Fig. 5, the honeycomb assemblies generated by scanning the potential in the range of ±1.00 V (Fig. 5c), ±1.50 V (Fig. 5b) are poor relative to that generated at ±2.00 V (Fig. 5a and Fig. 2). The honeycombs become tighter, bigger and well organized if the MWCNTs are pretreated in a high potential range, ±2.00 V. These assemblies (Fig. 5) demonstrate a better quality than those formed from untreated CNTs (Fig. 3) or treated by scanning the potential in positive or negative range only (Fig. 4). The threshold potential range should be ±1.50 V, beyond which the well defined honeycombs can be produced. It has been well reported that the oxidation threshold of CNTs to change their wetability to water is around 1.70 V [15], which agrees well with our value. When the potential range was smaller than this threshold, the electrochemical treatment of CNTs was not efficient and the honeycomb assembly was not well developed as illustrated in Fig. 5.

Since it has been observed that the deformation and tailoring of CNTs depend on the number of potential cycling [7,16], it is reasonable to control the honeycomb quality by varying the number of cycles. Such honeycomb structure control was exercised by extending the electrochemical treatment to 100 cycles and the results are shown in Fig. 6. As illustrated in Fig. 6a, the honeycombs obtained after 100 cycles are very different from those obtained after 50 potential cycles as shown in Fig. 2. The honeycombs exhibit larger nominal diameter and thinner rims as seen in Fig. 6a and its inset. The dominant distribution of the ejected charge on the top of the forest caused the highest leverage of the hydrophobicity and hydrophilicity of the top part of CNT forests and therefore the strongest interactions of neibouring CNTs as well as CNTs with the cations and latter with solvent molecule during evaporations. All those caused a thinner rim. The cavity depth is deeper than that in the Fig. 2 as shown in Fig. 6b and d. The structure stability was examined again by manipulating the freestanding rim cut away from the honeycomb cavity as shown in Fig. 6c. The structure stability in such thinner rims was still comparable to that of the thicker rims represented in Fig. 2. The structure difference can be seen more clearly in Fig. 6d, in which one single cavity was opened by FIB milling. In general, the bent MWCNT swirls in the cross-section were more compacted than those in Fig. 2d and were still the building blocks for combs. The CNTs right under the ridge were bent a little as well. The depth of this cavity was around 13 μm that is deeper than that (10 μm) in Fig. 2d. The thickness of the rim was determined to be only 300 nm in this cross-section view. Such super thin rims are desirable structures in real applications, such as field transition emitters [31] operated at low voltage or fuel cell electrodes to increase the catalyst load. This observation confirms the effectiveness of controlling the honeycomb structure by modulating the electrochemical parameters such as number of potential scanning cycles, scanning potential ranges etc. To get a good quality honeycomb, the electrochemistry shall be performed between +2.00 and −2.00 V for 50 to 100 cycles.

3.6. *Confocal Raman microspectroscopy*

Confocal Raman microspectroscopy is a powerful nondestructive approach for the characterization of crystallinity, morphology and chemical structures of various carbon allotropes as demonstrated for CNTs and graphene in single Raman spectra [32–37]. Raman spectroscopy was anticipated

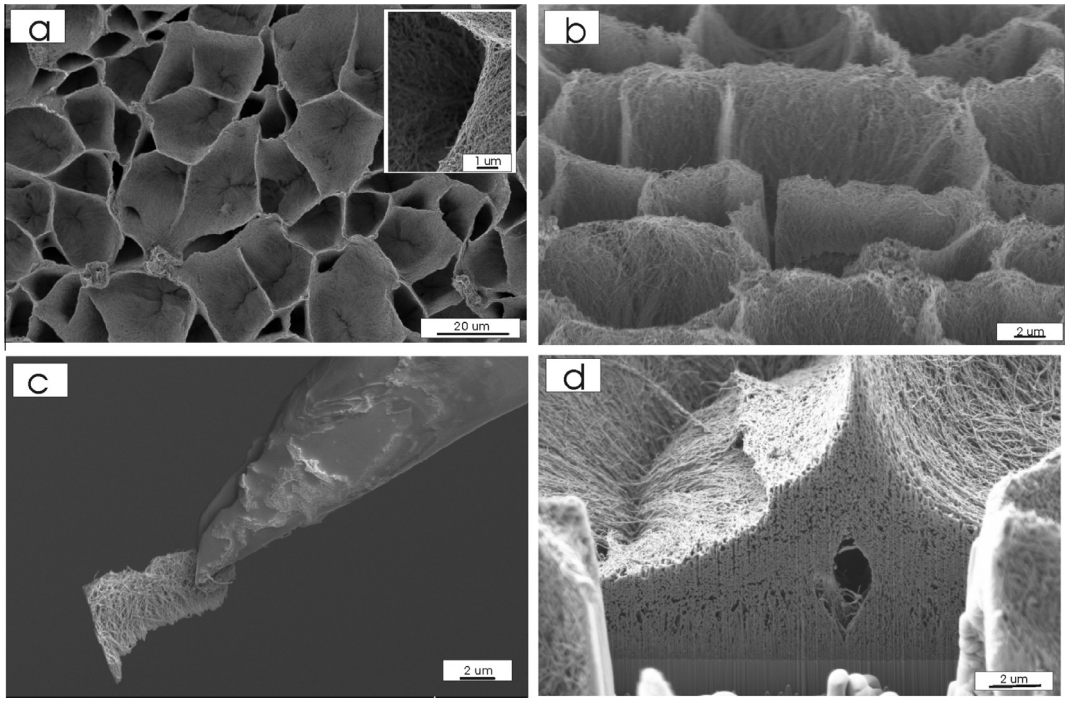

Fig. 6 – SEM images of honeycombs by capillary driving force exerting on the MWCNTs during the evaporation of the soaked liquid after 100 potential scanning cycles between −2.00 and 2.00 V. (a) A top view with an inset for an enlarged view of one comb; (b) a top view from a tilted angle; (c) mechanical manipulation of a comb rim; and (d) a side view of the comb rim.

to give new insight into the honeycomb structure, as shown elegantly by Tong and co-workers on the formation chemistry of chalcogenate-protected metal nanoparticles [38] and Dai's group on graphene unzipped from CNTs [37]. Here, we apply Raman spectroscopy to evaluate whether the physical, mechanical and electrical properties of CNTs are affected by the restructuring of CNT assembly. Fig. 7 shows the Raman image constructed using the G band intensity at 1590 cm^{-1} for each pixel. The G mode (1500–1600 cm^{-1}) with E_{2g} symmetry is due to the in-plane bond-stretching motion of pairs of C sp^2 atoms, which is characteristic of the graphite carbon (sp^2 sites) structure [34]. The Raman image clearly reproduces the honeycombs as seen in SEM image (Fig. 2), which confirms that the CNTs in honeycombs still maintain the graphite feature as in the original CNTs.

The pristine CNT and honeycomb formed after 100 cycles of potential scanning were further investigated by X-ray absorption near edge structure (XANES) spectroscopy (Fig. S1 in the Supplementary data). Two main peaks are clearly displayed at 285 and 291.2 eV for both samples. These can be attributed to the transitions from C 1s to unoccupied states of C–C π^* and C–C σ^* characters. The consistency of these two peaks in the two samples confirms that honeycomb retains carbon sp^2 (graphite) feature as the pristine CNTs [39]. Furthermore, a similar peak is observed in the two samples at ~288 eV that can be attributed to the carbonyl groups (e.g., carboxylates) resulting from the oxidation [40,41]. Dynamic potential cycling did not cause evident changes in surface function groups.

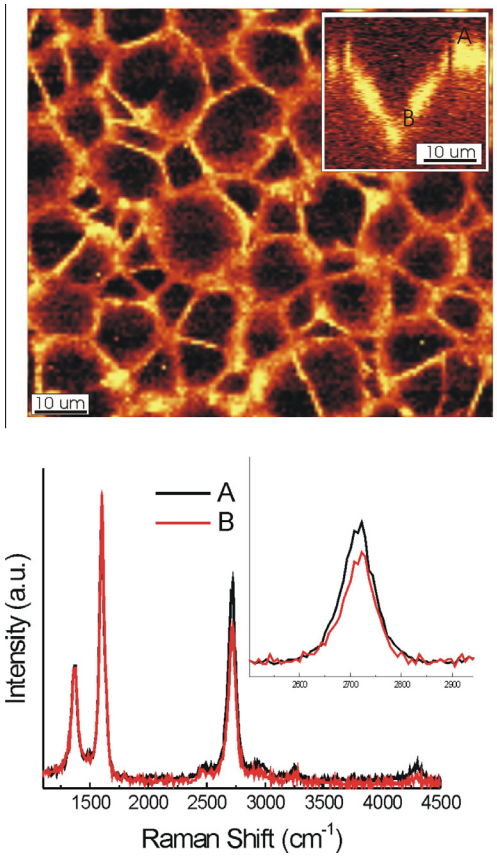

Fig. 7 – A typical Raman image of a honeycomb assembly constructed with the intensity of the graphite G band at 1590 cm^{-1} with 256 × 256 pixels. The Inset of the image is a depth scanning of one comb. Spectra A, B represent the Raman scattering at the top and bottom of the comb respectively. The spectrum inset is the enlarged G′ Raman band in spectra A and B.

The depth scan image shown in the inset in Fig. 7 reveals a single honeycomb cavity that demonstrates an inverted corn shape with an opening angle of 60–70°. More interestingly, the depth scan image in the Raman micrograph allows for probing the distribution of the chemical structure along the rim of the cavity. The Raman spectra corresponding to the top and the bottom of rims in the honeycomb are also displayed in Fig. 7. They showed three fundamental Raman scattering peaks at 1368, 1601 and ~2722 cm^{-1}, corresponding to the D, G and G′ or 2D vibration modes, respectively, of graphitic carbon. The D band at 1350 cm^{-1} is the breathing mode of six-fold aromatic rings with A_{1g} symmetry, which is forbidden in perfect graphite and only becomes active in the presence of disorder [34]. The D band intensity in spectra A and B showed little difference, which can be understood that the degree of structural disorder coming from spots A and B in the depth image is almost identical. Furthermore, the ratios of the D to G band intensities, used to evaluate the disorder structure density in carbon materials [33,34], were determined to be almost the same. The honeycomb assembling did not cause any extra disorder to MWCNTs. Considering the band positions, the CNTs in the honeycomb assembly is identical to the original CNTs, which again confirms the graphite feature within the honeycomb. Such conclusions also clarify the mild reaction feature of electrochemistry in contrast to the severe oxidation in strong acid treatment. Our MWCNTs in fact possess rolled graphene sheet structure as imaged previously [16]. Presumably excessive potential cycling would lead to the formation of carbon nanocrystals [7], the net result of the treatment in this study is to modify the overall CNT surface chemically, not drastically affecting the dominant characteristics. However the G′ band at 2722 cm^{-1} exhibits a noticeable difference for these two locations, spectra A and B in Fig. 7. The G' band or 2D band is the second order of zone boundary phonons, an overtone of the D mode [42], with a wavenumber about twice of that at D peak. Detail examination focused on this band can be conducted in the spectra in the inset of Fig. 7. It turns out that the band intensity is higher and the band peak moves to a lower wavenumber for MWCNTs at the top of rim than those at the cell bottom. The red shift was revealed clearly by the early rise of the G′ band from low wavenumber side (spectrum inset in Fig. 7). Such features can be attributed to less graphene layers for the MWCNTs at the top, leading to higher G′ peak intensity and lower wavenumbers. This interpretation was based on the observation on evolution of Raman spectra from graphite with a higher wavenumber to a single graphene layer with a lower wavenumber [42,43]. This observation was expected since the top of CNTs exhibits higher chemical activity and undergoes more serious oxidation [27] and deformation than their counterparts during the electrochemical treatment. The electrochemical reaction deforms and even opens CNTs along the wall [16], leading to thinner and flatter walls similar to graphene and therefore lower Raman shifts

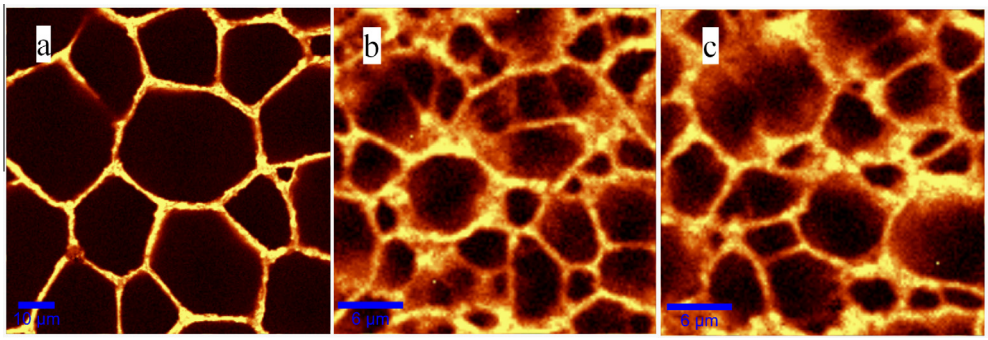

Fig. 8 – Comparison of Raman images on honeycombs formed from CNTs electrochemically treated by potential scanning in the range of ±2.00 V (a); ±1.50 V (b); and ±1.00 V (c) similar to Fig. 5. The images were constructed with the intensity of the graphite G band at 1590 cm^{-1} with 256 × 256 pixels. Other conditions are the same as in Fig. 7.

in G' peak position, higher peak intensity [42,43]. It was discovered that the disorder band intensity increased with further potential cycles (for instance, 1000 cycles) as illustrated by the ratio (I_D/I_G) of the D (1368 cm^{-1}) to G (1601 cm^{-1}) band intensities (see Fig. S2 in Supplementary data).

By means of Raman microspectroscopy, Fig. 8 demonstrates improved quality of the honeycomb assemblies generated by scanning the potential in the range of ±1.00 V, ±1.50 V and ±2.00 V. The cells become tighter, bigger and well organized if the MWCNTs are pretreated in a high potential range. The structural change tendency matches that observed from high resolution SEM as illustrated in Fig. 5. Again G′ peak position at cell ridges generated in wide potential range shifts to a little lower wavenumbers than that in narrow potential range.

4. Conclusions

A simple, low-cost but efficient method has been developed to fabricate a structurally stable array of multiwall carbon nanotubes with walled domains of honeycomb-like polygons via electrochemically modification. Structural tuning of the honeycomb structure was achieved by varying the potentiodynamic parameters such as potential scanning cycles, directions and ranges. The honeycomb structure thus obtained is robust and retains the structural characteristics of the pristine CNTs as revealed by the Raman imaging. The mechanisms for the honeycomb formation is associated with the capillary force induced by soaking and evaporating liquid in the mildly modified MWCNT forest, which is strong enough to bend CNTs against their elasticity as observed by high resolution SEM. The structure reported here is envisaged to become an important candidate material for potential applications in energy storage, catalytic support of fuel cells.

Acknowledgements

We appreciate the financial supports for this research from the Natural Sciences and Engineering Research Council of Canada (NSERC), Ontario Photonics Consortium (OPC), Canada Foundation for Innovation (CFI), Ontario Innovation Trust (OIT), the Premier's Research Excellence Award (PREA) and the University of Western Ontario.

Appendix A. Supplementary data

Supplementary data (X-ray absorption and Raman spectra of MWCNT before and after electrochemical treatments) associated with this article can be found, in the online version, at http://dx.doi.org/10.1016/j.carbon.2013.03.001.

REFERENCES

[1] Ge L, Sethi S, Ci L, Ajayan PM, Dhinojwala A. Carbon nanotube-based synthetic gecko tapes. Proc Natl Acad Sci USA 2007;104(26):10792–5.
[2] Iijima S. Helical microtubules of graphitic carbon. Nature 1991;354(6348):56–8.
[3] Frank S, Poncharal P, Wang ZL, de Heer WA. Carbon nanotube quantum resistors. Science 1998;280(5370):1744–6.
[4] Meng X, Geng D, Liu J, Li R, Sun X. Controllable synthesis of graphene-based titanium dioxide nanocomposites by atomic layer deposition. Nanotechnology 2011;22(16):165602/1–165602/10.
[5] Correa-Duarte MA, Wagner N, Rojas-Chapana J, Morsczeck C, Thie M, Giersig M. Fabrication and biocompatibility of carbon nanotube-based 3D networks as scaffolds for cell seeding and growth. Nano Lett 2004;4(11):2233–6.
[6] Alvarez NT, Hamilton CE, Pint CL, Orbaek A, Yao J, Frosinini AL, et al. Wet catalyst-support films for production of vertically aligned carbon nanotubes. ACS Appl Mater Interfaces 2010;2(7):1851–6.
[7] Zhou J, Booker C, Li R, Zhou X, Sham T-K, Sun X, et al. An electrochemical avenue to blue luminescent nanocrystals from multiwalled carbon nanotubes (MWCNTs). J Am Chem Soc 2007;129(4):744–5.
[8] Ye J-S, Liu X, Cui HF, Zhang W-D, Sheu F-S, Lim TM. Electrochemical oxidation of multi-walled carbon nanotubes and its application to electrochemical double layer capacitors. Electrochem Commun 2005;7(3):249–55.
[9] Fan JG, Dyer D, Zhang G, Zhao YP. Nanocarpet effect: pattern formation during the wetting of vertically aligned nanorod arrays. Nano Lett 2004;4(11):2133–8.
[10] Liu H, Li S, Zhai J, Li H, Zheng Q, Jiang L, et al. Self-assembly of large-scale micropatterns on aligned carbon nanotube films. Angew Chem Int Ed Engl 2004;43(9):1146–9.
[11] Lim XD, Foo HWG, Chia GH, Sow CH. Capillarity-assisted assembly of carbon nanotube microstructures with organized initiations. ACS Nano 2010;4(2):1067–75.

[12] Nguyen CV, Delzeit L, Cassell AM, Li J, Han J, Meyyappan M. Preparation of nucleic acid functionalized carbon nanotube arrays. Nano Lett 2002;2(10):1079–81.
[13] Chakrapani N, Wei B, Carrillo A, Ajayan PM, Kane RS. Capillarity-driven assembly of two-dimensional cellular carbon nanotube foams. Proc Natl Acad Sci USA 2004;101(12):4009–12.
[14] Li S, Li H, Wang X, Song Y, Liu Y, Jiang L, et al. Super-hydrophobicity of large-area honeycomb-like aligned carbon nanotubes. J Phys Chem B 2002;106(36):9274–6.
[15] Wang Z, Ci L, Chen L, Nayak S, Ajayan PM, Koratkar N. Polarity-dependent electrochemically controlled transport of water through carbon nanotube membranes. Nano Lett 2007;7(3):697–702.
[16] Zhou J, Cheiftz J, Li R, Wang F, Zhou X, Sham T-K, et al. Tailoring multi-wall carbon nanotubes for smaller nanostructures. Carbon 2009;47(3):829–38.
[17] Saha MS, Li R, Sun X. High loading and monodispersed Pt nanoparticles on multiwalled carbon nanotubes for high performance proton exchange membrane fuel cells. J Power Sources 2008;177(2):314–22.
[18] Yang D-Q, Sun S, Dodelet J-P, Sacher E. A facile route for the self-organized high-density decoration of Pt nanoparticles on carbon nanotubes. J Phys Chem C 2008;112(31):11717–21.
[19] Lefevre M, Proietti E, Jaouen F, Dodelet J-P. Iron-based catalysts with improved oxygen reduction activity in polymer electrolyte fuel cells. Science 2009;324(5923):71–4.
[20] Liu H, Zhai J, Jiang L. Wetting and anti-wetting on aligned carbon nanotube films. Soft Matter 2006;2(10):811–21.
[21] Liu H, Zhang Y, Aroto D, Li R, Merel P, Sun X. Aligned multi-walled carbon nanotubes synthesized by floating catalyst chemical vapor deposition: effects of buffer layer. Surf Coat Technol 2008;202:4114–20.
[22] Bard AJ, Faulkner LR. Electrochemical methods: fundamentals and applications. 2nd ed. New York: John Wiley; 2001.
[23] Wang F, Zhou X, Zhou J, Sham T-K, Ding Z. Observation of single tin dioxide nanoribbons by confocal Raman microspectroscopy. J Phys Chem C 2007;111(51):18839–43.
[24] Bico J, Roman B, Moulin L, Boudaoud A. Adhesion: elastocapillary coalescence in wet hair. Nature 2004;432(7018):690.
[25] Fang H-T, Liu C-G, Liu C, Li F, Liu M, Cheng H-M. Purification of single-wall carbon nanotubes by electrochemical oxidation. Chem Mater 2004;16(26):5744–50.
[26] Ito T, Sun L, Crooks RM. Electrochemical etching of individual multiwall carbon nanotubes. Electrochem Solid-State Lett 2003;6(1):C4–7.
[27] Banks CE, Davies TJ, Wildgoose GG, Compton RG. Electrocatalysis at graphite and carbon nanotube modified electrodes: edge-plane sites and tube ends are the reactive sites. Chem Commun 2005;7:829–41.
[28] Wildgoose GG, Hyde ME, Lawrence NS, Leventis HC, Jiang L, Jones TGJ, et al. 4-Nitrobenzylamine partially intercalated into graphite powder and multiwalled carbon nanotubes: characterization using X-ray photoelectron spectroscopy and in situ atomic force microscopy. Langmuir 2005;21(10):4584–91.
[29] Wildgoose GG, Wilkins SJ, Williams GR, France RR, Carnahan DL, Li J, et al. Graphite powder and multiwalled carbon nanotubes chemically modified with 4-nitrobenzylamine. ChemPhysChem 2005;6(2):352–62.
[30] Zhao YP, Fan JG. Clusters of bundled nanorods in nanocarpet effect. Appl Phys Lett 2006;88(10):103123/1–3.
[31] Fan S, Chapline MG, Franklin NR, Tombler TW, Cassell AM, Dai H. Self-oriented regular arrays of carbon nanotubes and their field emission properties. Science 1999;283(5401):512–4.
[32] Ferrari A, Robertson J. Raman spectroscopy of amorphous, nanostructured, diamond-like carbon, and nanodiamond. Phil Trans R Soc Lond A 2004;362(1824):2477–512.
[33] Dresselhaus MS, Dresselhaus G, Saito R, Jorio A. Raman spectroscopy of carbon nanotubes. Phys Rep 2005;409(2):47–99.
[34] Ferrari AC, Robertson J. Interpretation of Raman spectra of disordered and amorphous carbon. Phys Rev B 2000;61(20):14095–107.
[35] Cong C, Yu T, Saito R, Dresselhaus GF, Dresselhaus MS. Second-order overtone and combination Raman modes of graphene layers in the range of 1690–2150 cm^{-1}. ACS Nano 2011;5(3):1600–5.
[36] Piao Y, Chen C-F, Green AA, Kwon H, Hersam MC, Lee CS, et al. Optical and electrical properties of inner tubes in outer wall-selectively functionalized double-wall carbon nanotubes. J Phys Chem Lett 2011;2(13):1577–82.
[37] Xie L, Wang H, Jin C, Wang X, Jiao L, Suenaga K, et al. Graphene nanoribbons from unzipped carbon nanotubes: atomic structures, Raman spectroscopy, and electrical properties. J Am Chem Soc 2011;133(27):10394–7.
[38] Li Y, Zaluzhna O, Xu B, Gao Y, Modest JM, Tong YJ. Mechanistic insights into the Brust-Schiffrin two-phase synthesis of organo-chalcogenate-protected metal nanoparticles. J Am Chem Soc 2011;133(7):2092–5.
[39] Zhou J, Zhou X, Sun X, Li R, Murphy M, Ding Z, et al. Interaction between Pt nanoparticles and carbon nanotubes – an X-ray absorption near edge structures (XANES) study. Chem Phys Lett 2007;437(4–6):229–32.
[40] Zhou J, Wang J, Liu H, Banis MN, Sun X, Sham T-K. Imaging nitrogen in individual carbon nanotubes. J Phys Chem Lett 2010;1(11):1709–13.
[41] Zhou JG, Fang HT, Maley JM, Ko JYP, Murphy M, Chu Y, et al. An X-ray absorption, photoemission, and Raman study of the interaction between SnO_2 nanoparticle and carbon nanotube. J Phys Chem C 2009;113(15):6114–7.
[42] Graf D, Molitor F, Ensslin K, Stampfer C, Jungen A, Hierold C, et al. Spatially resolved Raman spectroscopy of single- and few-layer graphene. Nano Lett 2007;7(2):238–42.
[43] Ferrari AC, Meyer JC, Scardaci V, Casiraghi C, Lazzeri M, Mauri F, et al. Raman spectrum of graphene and graphene layers. Phys Rev Lett 2006;97(18):187401/1–4.